

Article

Fatigue Life Prediction of CFRP-Strengthened RC Beams with Flexural Crack under Hygrothermal Environments

Xinyan Guo ¹, Hangyue Cui ¹, Yilin Wang ² and Zhanbiao Chen ^{1,*}

¹ School of Civil Engineering and Transportation, South China University of Technology, Guangzhou 510640, China; xyguo@scut.edu.cn (X.G.); 202120107677@mail.scut.edu.cn (H.C.)

² Magnel–Vandepitte Laboratory, Department of Structural Engineering and Building Materials, Ghent University, Technologiepark—Zwijnaarde 60, 9052 Ghent, Belgium; yilin.wang@ugent.be

* Correspondence: chenzb@scut.edu.cn

Abstract: The durability of reinforced concrete (RC) beams strengthened with carbon fiber-reinforced polymer (CFRP) is a worldwide concern in structural engineering. As an important part of the strengthened beam, the performance of the CFRP–concrete interface under hygrothermal environments is a delicate problem. In this paper, the fatigue behavior of CFRP-strengthened RC beams is analyzed by a theoretical model. In the model, CFRP–concrete interface degradation under hygrothermal environments is involved. Since interface debonding and rebar fracture induced by intermediate cracking are two typical failure modes, the damage models of rebar and the CFRP–concrete interface are established. Based on the theoretical model, the failure mode of CFRP-strengthened RC beams can be predicted, and fatigue life can be determined. The results showed that IC debonding is more likely to occur under hygrothermal environments. The accurate prediction of failure modes is essential for fatigue life prediction.



Citation: Guo, X.; Cui, H.; Wang, Y.; Chen, Z. Fatigue Life Prediction of CFRP-Strengthened RC Beams with Flexural Crack under Hygrothermal Environments. *Materials* **2022**, *15*, 4681. <https://doi.org/10.3390/ma15134681>

Academic Editors: Xianjun Pei, Pasqualino Corigliano and Haibo Yang

Received: 30 May 2022

Accepted: 27 June 2022

Published: 4 July 2022

Publisher's Note: MDPI stays neutral with regard to jurisdictional claims in published maps and institutional affiliations.



Copyright: © 2022 by the authors. Licensee MDPI, Basel, Switzerland. This article is an open access article distributed under the terms and conditions of the Creative Commons Attribution (CC BY) license (<https://creativecommons.org/licenses/by/4.0/>).

Keywords: CFRP; CFRP–concrete interface; failure mode; life prediction; RC beam

1. Introduction

Existing reinforced concrete (RC) structures have become weak and dilapidated due to various factors, including vehicle growth, population explosion, and extreme environmental erosion. Fiber-reinforced polymer (FRP) composites have high tensile strength, low self-weight, and good corrosion resistance and have been extensively used to strengthen and rehabilitate RC bridge structures over the past decades [1–3].

There are considerable studies on the static behavior of FRP-strengthened RC beams [4–6]. In response to higher demand for sustained loads from pedestrians and vehicles, it is necessary to take into consideration the fatigue behavior of the strengthened beams. However, limited fatigue testing has been carried out [7–9]. B.G. Charalambidi [7] found that bonding FRP could provide the residual capacity of RC beams after rebar fracture, and the stiffness ratio of rebar to FRP was crucial to the fatigue behavior of FRP-strengthened beams. The fatigue life was controlled mainly by rebars. R. Al-Rousan [8] studied the fatigue behavior of CFRP-strengthened beams with nonlinear finite element analysis and found that the secant stiffness degraded due to fatigue loading. Stiffness degradation under fatigue loading is an important manifestation of cumulative fatigue damage. However, researchers assumed that there was a perfect bond between FRP and concrete, which was not inconsistent with the actual constructional engineering [7–9]. The failure modes of FRP-strengthened RC beams also include the debonding of the FRP–concrete interface. In E. Ferrier's research [10], a slipping effect was involved in the RC beam section equilibrium that was analyzed by the delay characteristics of each constituent material. In particular, the relationship that exists between the strain and shear stress for the FRP–concrete interface was added to the theoretical model. The partly cohesive debonding in the concrete was the main reason for the failure of the RC beam. There was still a drawback in that the softening stage of the

relationship between FRP and concrete was not involved. Therefore, a more appropriate bond–slip relationship should be used in this area.

The interfacial behavior of the FRP–concrete interface under monotonic loading has been investigated [11–13], and bond–slip models have been proposed [14–17]. Debonding failure of the FRP–concrete interface is regarded as one of the main failure modes after quasi-static loading. In comparison, the findings under fatigue loading are limited, such as the influence of concrete crack [18], stress distribution on FRP [19], and the bond–slip relationship of the FRP–concrete interface [19–21]. A. Al-Saoudi [18] simulated the cracking of concrete close to FRP under fatigue loading by FEA and proposed a crack softening law. The crack opening displacement was used as the criterion to judge the interface failure. H. Diab [22] incorporated Maxwell’s constitutive model into the FE model and found that the stress on FRP was redistributed due to the effect of fatigue loading, leading to an increase in the effective bond length with increasing loading cycles. K.Y.M. Loo [20] considered the bilinear bond–slip model in the FE model and assumed that the stiffness of the FRP–concrete interface was constant during the fatigue loading process. The bond strength was exhausted due to fatigue loading, which caused local debonding of the FRP–concrete interface. As a result, the peak stress under fatigue loading moved along the length until the peak stress under static loading could not be maintained. Since the fatigue failure models of FRP-strengthened RC beams include concrete crack propagation, rebar rupture, and interface debonding, the concrete crack length, damage to rebar and the FRP–concrete interface, and stiffness degradation should be considered in the failure criteria. Thus, it is quite significant to apply an appropriate theory to the failure criterion.

Bridges are serviced in various extreme environments, such as salt spray [23], hot and humid [24,25], freeze–thaw [26], ultraviolet radiation [27], and wet/dry circulation [28] environments, so it is necessary to study environmental effects on FRP-strengthened RC beams. The study of the FRP–concrete interface plays a significant role, because the interface is sensitive to environments. The epoxy resin of FRP composite is greatly influenced by temperature and humidity [29]. Zheng [30] carried out double-shear experiments on FRP–concrete interfaces under a simulated hygrothermal environment (60 °C, 95% R.H). The results indicated that the high-temperature and -humidity environment obviously decreased the interfacial stiffness. The influence of elevated service temperature (20, 50, 65, and 80 °C) on the bonding performance of the FRP–concrete interface was studied [31]. There was a relative decrease in fatigue performance with an increase in temperature. Additionally, it was found that the bond failure was characterized by a thin layer of concrete on FRP sheets under 50 and 65 °C but almost no concrete under 80 °C. Therefore, there are two interfacial failure modes: cohesive failure and adhesive failure. Adhesive failure tends to be predominant at high temperatures. To further analyze the interfacial failure criteria under elevated temperature, Dai [32] proposed the interfacial brittleness index and interfacial fracture energy determined by regression analysis of test data.

Finally, it is necessary to take into consideration the coupling effect of fatigue load and hygrothermal conditions on fatigue behavior of FRP-strengthened RC beams. Based on Huang’s results [33], Qin [34] established a fatigue life prediction model of FRP-strengthened beams subjected to fatigue load and a hygrothermal environment. The effects of temperature and relative humidity were considered as material coefficients, determined by regression analysis of test data. However, the critical part—the FRP–concrete interface—was not considered in these studies. Therefore, the failure mechanism of FRP-strengthened beams under fatigue load and a hygrothermal environment has not been clarified.

With a focus on the durability of CFRP-strengthened RC beams, a theoretical model considering the degradation of the CFRP–concrete interface under hygrothermal environments was proposed. With this model, the accumulated damage of strengthened beams with intermediate flexural crack was analyzed. According to the analysis, two main failure modes were considered: IC debonding and rebar fracture caused by the intermediate crack. Moreover, two corresponding failure criteria were established. The proposed theoretical

model and calculation procedure can be used to predict the failure mode of strengthened beams and determine the fatigue life under hygrothermal environments.

2. Fatigue Life Prediction Model of Mid-Span Cracked Beam

During the fatigue process, the properties of RC beams degrade because of the concrete cumulative damage. RC beams are vulnerable to cracking because of the low tensile strength of concrete. In the preliminary studies of this research group [33–35], a typical failure mode of CFRP-strengthened RC beams was found which shows that one main type-I crack propagates with cyclic loads and finally leads to the failure. Therefore, this paper considered the situation of a CFRP-strengthened beam with an intermediate flexural crack under constant amplitude fatigue load. The mid-span deflection, shear stress distribution, and interfacial crack length changed as the loading cycle increased.

2.1. Interfacial Shear Stress Distribution

Several model types are suitable for the description of the interfacial bond–slip relationship, such as the bilinear, cutoff, elastic–plastic, and Popovics models [36]. Because of the good approximation of the interfacial non-linear relationship, the bilinear model is used in this paper. In the bilinear bond–slip model, three phases, including elasticity, softening, and debonding, are considered and presented:

$$\tau(s) = \begin{cases} k_1 s; & 0 < s \leq s_0 \\ k_2 (s_u - s); & s_0 < s \leq s_u \\ 0; & s > s_u \end{cases} \quad (1)$$

where s is the slip along the CFRP–concrete interface; s_0 is the interfacial slip corresponding to shear strength τ_u ; s_u is the interfacial debonding slip; $k_1 = \frac{\tau_u}{s_0}$ is the slope in the elastic phase; and $k_2 = \frac{\tau_u}{s_u - s_0}$ is the slope in the softening phase.

To study the influence of humidity and temperature variations on CFRP–concrete interface degradation, Zheng [37] conducted shear testing on concrete blocks externally bonded with CFRP. All specimens were exposed to an accelerated hygrothermal environment for 14 days. Degradation of the CFRP–concrete interface was significant compared to specimens without environmental pretreatment, especially with the effect of temperature. Bilinear bond–slip models were established with the tested bond parameters from Zheng’s results [37], as shown in Figure 1. The adapted parameters are listed in Table 1.

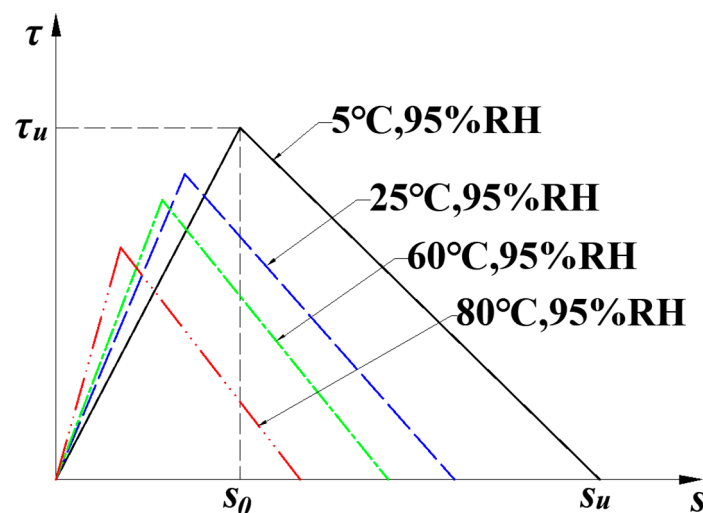


Figure 1. Bilinear bond–slip relationship with different hygrothermal pretreatments.

Table 1. Major bond parameters for bond–slip relationship with different hygrothermal pretreatments (data from [37]).

Hygrothermal Conditions	τ_u (MPa)	s_0 (mm)	s_u (mm)	k_1	k_2	G_f
5 °C, 95% R·H	4.25	0.055	0.266	77.3	15.9	0.515
20 °C, 95% R·H	3.46	0.036	0.174	96.1	19.9	0.176
50 °C, 95% R·H	3.05	0.030	0.143	101	21.3	0.094
80 °C, 95% R·H	2.53	0.019	0.096	133	26.4	0.054

2.2. Time-Dependent Characters of Concrete

Because of its perfect fatigue resistance, CFRP has been considered a kind of linear elastic material in the whole fatigue process, but the concrete effective modulus E_{ci} at the i th cycle degrades because of cumulative damage [38], which can be calculated by [39]:

$$E_{ci} = \left(1 - 0.33 \frac{n_i}{N_{ci}} \right) E_c \tag{2}$$

where n_i is the cycle number; E_c is the initial elastic modulus; and N_{ci} is the fatigue life corresponding to compressive stress, which can be calculated by [39]:

$$S_{ci} = 0.9885 - 0.0618 \lg N_{ci} \tag{3}$$

where S_{ci} is the ratio of the compressive stress σ_{ci} to the uniaxial strength f_c at the i th cycle.

The main rebar in this paper is assumed to be elastoplastic. The rebar keeps linear elasticity before yielding, and when the tensile stress σ_s is higher than the yield stress, it keeps constant at yield stress.

2.3. Properties at Mid-Span Section under Constant Amplitude Fatigue Load

Figure 2 shows the typical cross-section character of a simple-supported CFRP-strengthened RC beam under cyclic fatigue load.

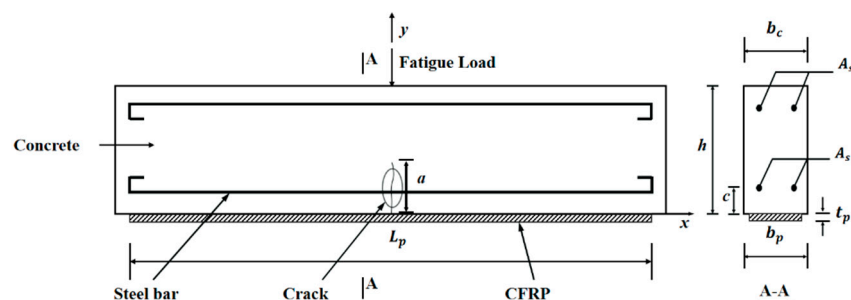


Figure 2. CFRP-strengthened RC beam with mid-span crack.

Figure 3 shows the mid-span section of the strengthened beam under fatigue loading. As the number of cycles i increases, the degradation in concrete elastic modulus E_{ci} causes many changes, such as crack length a_{0i} , the neutral axis location h_{c0i} , and the curvature ρ_{0i} . Assuming that the cross-section strain is linear, Figure 3 shows the distribution of stress-strain at the mid-span section. The equilibrium equations can be established as follows:

$$\begin{cases} A_s \sigma_{s0i} + b_p t_p E_p \left[\frac{(h_{c0i})}{\rho_{0i}} + \delta'_i(0) \right] + b E_{ct} \frac{(h_{c0i} - a_{0i})^2}{2\rho_{0i}} = b E_{ci} \frac{(h - h_{c0i})^2}{\rho_i} + A'_s E'_s \frac{(h - h_{c0i} - c)}{\rho_i} \\ A_s \sigma_{si}(h_{ci} - c) + b_p t_p E_p h_{c0i} \left[\frac{(h_{c0i})}{\rho_{0i}} + \delta'_i(0) \right] + b E_{ct} \frac{(h_{ci} - a_i)^3}{3\rho_{0i}} + b E_{ci} \frac{(h - h_{c0i})^3}{2\rho_{0i}} + A'_s E'_s \frac{(h - h_{c0i} - c)^2}{\rho_{0i}} = M \end{cases} \tag{4}$$

where M is the flexural moment; b_p and b are the width of the CFRP and the beam, respectively; A_s and A'_s are the cross-section areas of tension- and compression-rebar,

respectively; h is the height of the RC beam; c is the concrete cover thickness; t_p is the thickness of the CFRP; and E_p , E_c , and E_s' are the elastic moduli of the CFRP, concrete in tension, and rebar in compression, respectively.

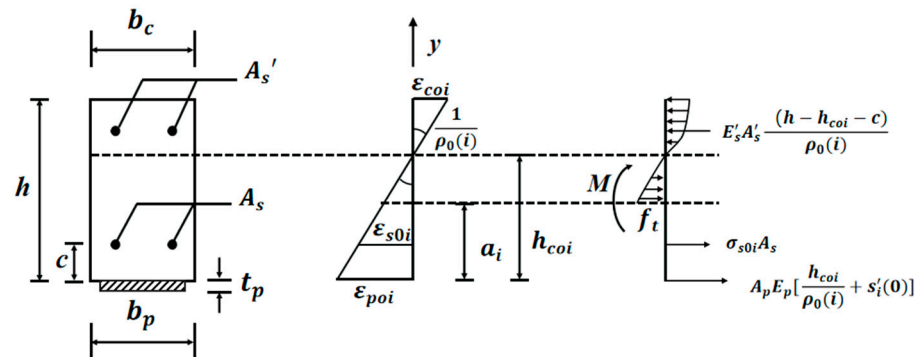


Figure 3. Distribution of stress-strain at the mid-span section.

In Equation (4), the first derivative of the interface slips at mid-span $s_i'(x)$ is established as follows:

$$s_i'(x) = \varepsilon_{pi}(x) - \varepsilon_{ci}(x) \tag{5}$$

where $\varepsilon_{pi}(x)$ and $\varepsilon_{ci}(x)$ are the strains of the CFRP and the concrete at the bottom of the RC beam, respectively.

Since the behavior of the CFRP–concrete interface is different in the elastic and softening phases, the interfacial slip and stress should be discussed separately. During the elastic stage, the interfacial stress τ does not reach τ_u ; then, the interfacial slip $s_i(x)$ is expressed as [35]:

$$s_i(x) = A \left(e^{x\lambda(i)\sqrt{k_1}} + e^{-x\lambda(i)\sqrt{k_1}} \right) \tag{6}$$

where $\lambda(i) = \sqrt{\frac{1}{E_p \cdot t_p} + \frac{b_p}{E_c(i) \cdot b \cdot h}}$ and $A = \frac{-2\lambda(i)t_p \cdot \sigma_{p0i} \cdot e^{\lambda(i)\frac{L_p}{2}} \sqrt{k_1}}{\sqrt{k_1} \cdot (e^{\lambda(i)L_p \sqrt{k_1}} - 1)}$.

Once τ reaches the maximum shear stress τ_u , then the interface is in the softening stage. The interfacial slip $s_i(x)$ in the softening stage is:

$$s_i(x) = B \cos [x\lambda(i)\sqrt{k_2}] + C \sin [x\lambda(i)\sqrt{k_2}] + s_u \tag{7}$$

B and C are constants which can be determined by boundary and continuous conditions [35].

At the tip of the intermediate crack, the tensile stress of concrete reaches uniaxial tensile strength f_{ct} :

$$E_{ct} \frac{h_{c0i} - a_i}{\rho_{0i}} = f_{ct} \tag{8}$$

Because the tensile rebar is considered ideal elastoplastic, the expression of the tensile stress σ_{s0i} at each cycle is:

$$\sigma_{s0i} = \begin{cases} E_s \varepsilon_{s0i}, & \varepsilon_{s0i} < \varepsilon_y \\ f_y, & \varepsilon_{s0i} > \varepsilon_y \end{cases} \tag{9}$$

where E_s is the elastic modulus; ε_y is the yield strain; and ε_{s0i} is the axial strain of the tensile rebar at the i th cycle, which can be given by:

$$\varepsilon_{s0i} = \frac{(h_{c0i} - c)}{\rho_{0i}} \tag{10}$$

From the Equations (4)–(10), the intermediate crack length a_i , the neutral axis height h_{c0i} , and the curvature $\frac{1}{\rho_{0i}}$ can be determined. Meanwhile, at the i th cycle, the deflection v_{0i} at mid-span can be expressed as:

$$v_{0i} = \frac{PL^3}{48M\rho_i(0)} \quad (11)$$

2.4. Failure Criterion

Fatigue tests on CFRP-strengthened RC beams have been carried out in preliminary research [40–42]. Results showed that there were several failure modes, including tensile rebar fracture, CFRP–concrete interface debonding, and compressive concrete crushing. Tensile rebar rupture at mid-span and CFRP–concrete interface debonding always occurred, especially under hygrothermal environments. Moreover, these two failure modes may occur simultaneously. However, which failure will occur first is difficult to predict. Therefore, a fatigue life prediction method considering failure modes is discussed in this section.

2.4.1. Cumulative Damage Model of Rebar

As described in Section 2.3, with the increase in loading cycles, the tensile stress of rebar increases because of the modulus degradation of concrete. A typical S – N relationship [43] of rebar is involved:

$$\log N_i = \begin{cases} 8.460 - 0.011S_{si}, & 420.5 < S_{si} \leq 787.7 \\ 47.96 - 0.105S_{si}, & 411.0 < S_{si} \leq 420.5 \\ 7.578 - 0.006S_{si}, & 251.6 < S_{si} \leq 411.0 \\ 10.29 - 0.017S_{si}, & 192.2 < S_{si} \leq 251.6 \end{cases} \quad (12)$$

where S_{si} is the amplitude of applied tensile stress in MPa and N_i is the fatigue life of rebar corresponding to S_{si} .

By using Miner's rule, the cumulative damage of rebar D_s can be calculated:

$$D_s = \sum \frac{n_i}{N_i} \quad (13)$$

where n_i is the cycle number of rebar at the stress amplitude S_{si} .

Based on Equations (9) and (10), S_{si} can be calculated at peak and valley loads. During the computing process, when the cumulative damage D_s reaches 1, the rebar fractures.

2.4.2. Cumulative Damage of CFRP–Concrete Interface

The debonding failure of strengthened RC beams can be divided into two types: intermediate crack (IC) failure and plate end (PE) failure. Due to the existence of strain difference at the CFRP end, PE failure occurs after the separation of CFRP from concrete. Meanwhile, IC debonding failure initiates from the intermediate crack at the mid-span of the beam; this is because the higher interfacial shear stress is around the intermediate crack [44].

PE debonding failure needs to be considered when there is no intermediate crack. To avoid such a debonding failure, it is effective to anchor the end of the CFRP. However, flexural cracks always appear at the mid-span of strengthened RC beams, which increases the possibility of IC debonding failure. Thus, IC debonding failure needs to be involved in this study.

The energy release rate in the CFRP–concrete interface under the flexural moment G_R can be expressed as [45]:

$$G_R = \frac{1}{b_p} \left[\left| \frac{\partial W_{ext}}{\partial a} \right| - \left| \frac{\partial W_{sys}}{\partial a} \right| \right] \quad (14)$$

where $\frac{\partial W_{ext}}{\partial a}$ is the changing rate of the work performed by external force; $\frac{\partial W_{sys}}{\partial a}$ is the changing rate of the energy dissipated caused by moment-curvature and CFRP strain; and ∂a is the length increment of the interfacial crack.

In Equation (15), the changing rate of the work performed by external force is:

$$\frac{\partial W_{ext}}{\partial a} = \frac{P\Delta v}{\Delta a} \quad (15)$$

where P is the external load; Δa is the length increment of the interfacial crack; and Δv is the deflection increment at the loading point.

The changing rate of dissipated energy $\frac{\partial W_{sys}}{\partial a}$ includes the work performed on the CFRP (ΔW_p) and on the RC beam (ΔW_b).

$$\Delta W_b = \frac{1}{2}(M_{1a} + M_{2a}) \left(\frac{1}{\rho_2(x)} - \frac{1}{\rho_1(x)} \right) \quad (16)$$

$$\Delta W_p = \frac{1}{2}b_p t_p (\sigma_{1p} + \sigma_{2p}) (\varepsilon_{2p} - \varepsilon_{1p}) \quad (17)$$

where the subscripts 1 and 2 represent the states before and after the debonding crack of the CFRP–concrete interface, respectively; M_{1a} and M_{2a} are the corresponding flexural moments; $\frac{1}{\rho_2(x)}$ and $\frac{1}{\rho_1(x)}$ are the corresponding curvatures; F_{1p} and F_{2p} are the corresponding CFRP tensile forces; and ε_{2p} and ε_{1p} are the corresponding CFRP tensile strains.

If $G_R \geq G_f$, IC debonding failure occurs according to the failure criteria. The failure fracture G_f is different under various hygrothermal environments, and the values are listed in Table 1.

2.5. Calculation Procedure

Based on the prediction model, the fatigue life of CFRP-strengthened RC beams can be calculated. Figure 4 describes the implementation steps for predicting failure modes and the corresponding fatigue life. The details are as follows:

The dimensions and material parameters of the strengthened beam are inputted into the theoretical model.

The bond–slip relationships under different environments and fatigue loads are inputted into the theoretical model.

The peak and valley values of cyclic loads are inputted into the theoretical model. From the previous step, the degraded elastic modulus and compression stress of concrete can be obtained by Equations (2) and (3). The parameters of the concrete after degradation are entered in the next step.

The curvature $\frac{1}{\rho_{0i}}$, the rebar stress σ_{s0i} , the deflection v_{0i} , and the concrete compressive stress σ_{c0i} at the intermediate cracked section can be determined in each step (Section 2.3).

In each step, the cumulative damage to rebar D_s (Section 2.4.1) can be obtained. If D_s reaches 1, rebar rupture will be the main failure mode, and the corresponding loading cycle number i will be the predicted fatigue life.

The shear stress distribution can be obtained (Section 2.1). When the interfacial bonding slip reaches s_u , the interfacial crack will propagate. Then, the interface crack increment ∂a can be obtained.

From the theory involved in Section 2.3, $\frac{\Delta W_b}{\partial a}$, $\frac{\Delta W_p}{\partial a}$, and G_R are determined.

If $G_R \geq G_f$, the failure mode will be IC debonding, and the corresponding loading cycle number i will be the predicted fatigue life.

As long as either one of the cumulative damages, D_s or D_b , reaches 1, the corresponding failure mode will occur first.

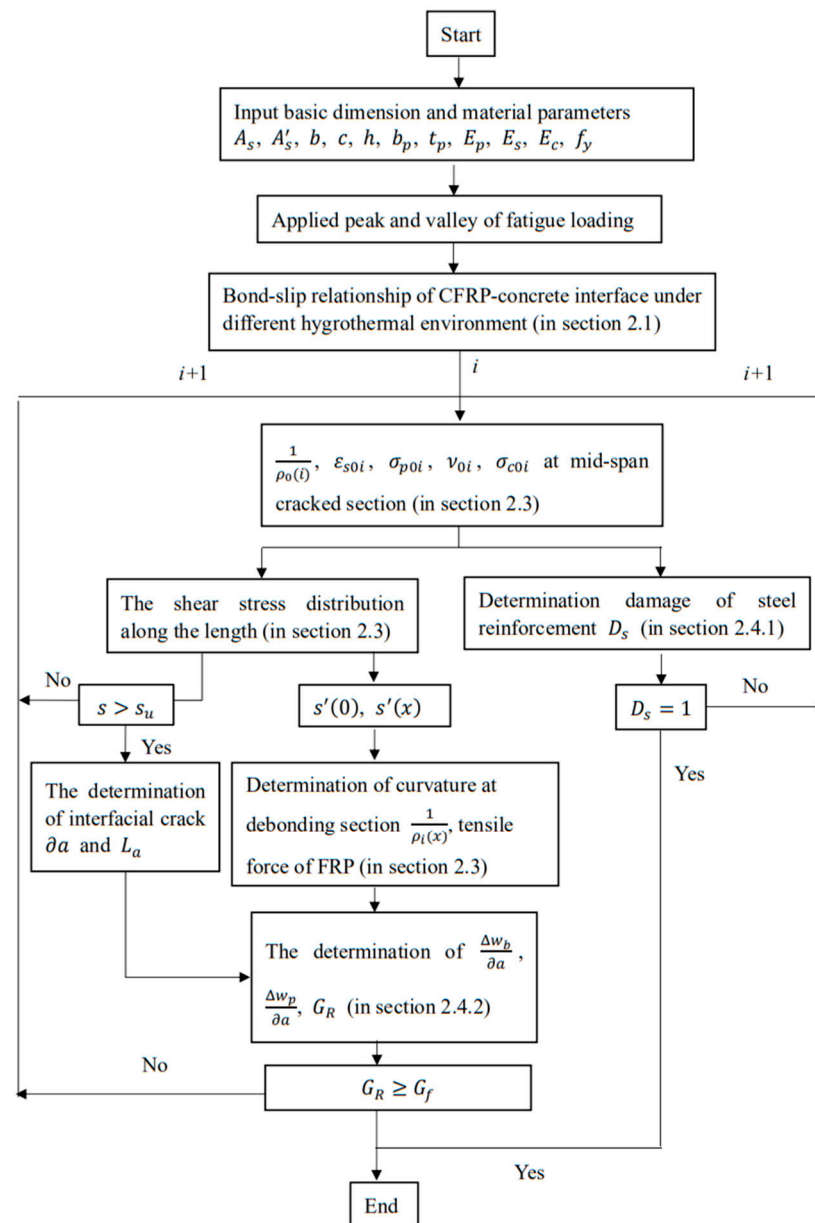


Figure 4. Flowchart for calculation procedure.

3. Results and Discussions

To verify the effect of the hygrothermal environment on strengthened beams' fatigue performance, numerical examples for strengthened beams were proposed. At a constant relative humidity of 95%, temperatures varied from 5 °C to 80 °C. Then, the distribution of interfacial stress and failure mode changed accordingly. The predicted fatigue lives corresponding to each failure mode were calculated.

The major parameters of bond–slip relationships with and without hygrothermal pretreatments are listed in Table 1. Regarding the numerical calculations, the parameters of materials and geometric features listed in Tables 2 and 3 are similar to those used by Qin [34] and Wang [43]. Under hygrothermal environments, the failure mode of rebar rupture or IC debonding can be predicted according to the failure criteria. Moreover, the corresponding fatigue lives of strengthened beams were also predicted and compared with the test results.

Table 2. Parameters of RC beam strengthened by CFRP.

E_p (GPa)	E_c (GPa)	E_s (GPa)	E'_s (GPa)	f_c (MPa)	f_{ct} (MPa)	f_y (MPa)
230	34	206	206	47.6	4.45	400

Table 3. Geometric features of RC beam strengthened by CFRP.

b (mm)	h (mm)	L (mm)	L_p (mm)	t_p (mm)	b_p (mm)	c (mm)	A_s (mm ²)	A'_s (mm ²)
100	200	1850	1560	0.23	100	30	157	100

3.1. Deflection of the Mid-Span Section

Figure 5 shows the deflections versus loading cycles before D_s reaches 1 under different hygrothermal environments. The maximum deflection increases with increasing temperature. The reason for stiffness degradation is that the slope for the bond–slip relationship at the interface changes when exposed to various hygrothermal environments. For specimens at a peak fatigue load of 27.5 kN (Figure 5a), the corresponding maximum mid-span deflections under hygrothermal environments of 5 °C, 20 °C, 50 °C, and 80 °C are 4.35 mm, 4.65 mm, 5.35 mm, and 5.62 mm, respectively. For specimens at a peak fatigue load of 30.0 kN (Figure 5b), the corresponding maximum mid-span deflections under hygrothermal environments of 5 °C, 20 °C, 50 °C, and 80 °C are 4.85 mm, 5.39 mm, 5.35 mm, and 6.15 mm, respectively. Moreover, under the same hygrothermal environment, the maximum deflection increases with the increase in peak fatigue load.

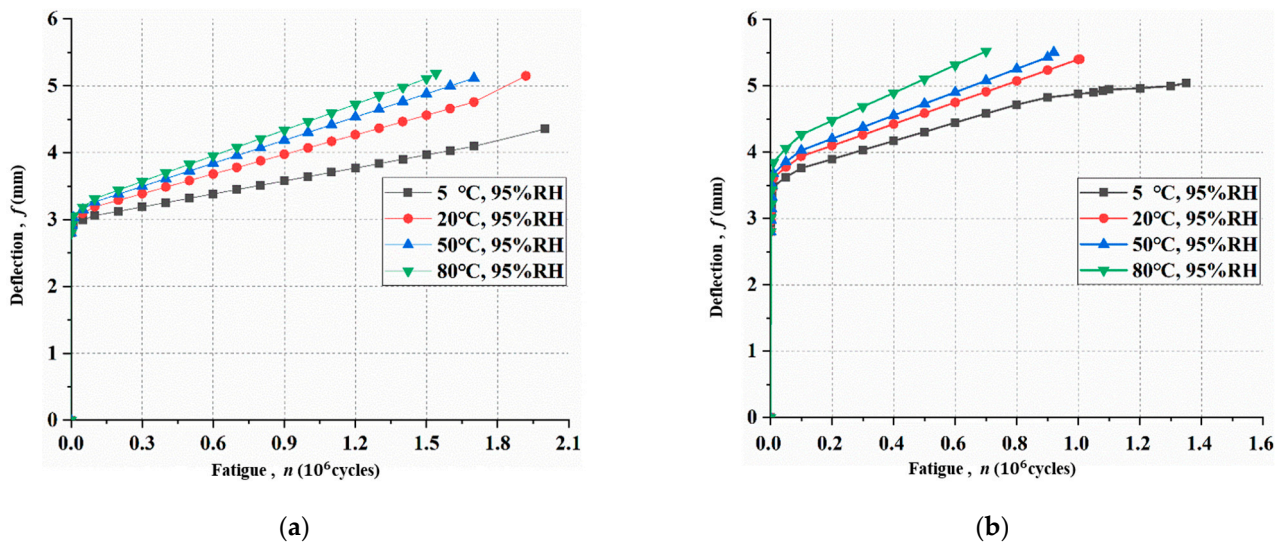


Figure 5. Maximum deflections under different fatigue loads and hygrothermal environments: (a) 27.5 kN; (b) 30.0 kN.

3.2. Cumulative Damage of Rebar

Based on the calculation procedure, the tensile stress and cumulative damage of rebar D_s at different cycles can be derived by Equations (12) and (13). The cumulative damage of rebar D_s versus loading cycles under different hygrothermal environments is shown in Figure 6. As shown in Figure 6a, D_s did not reach 1 at two million loading cycles under hygrothermal conditions of 5 °C, 95% R-H. With the increase in temperature, D_s grows rapidly because of the increase in mid-span deflection caused by the effect of the hygrothermal environment. Furthermore, it was also observed from Figure 6 that the D_s increased with the increase in fatigue loading level.

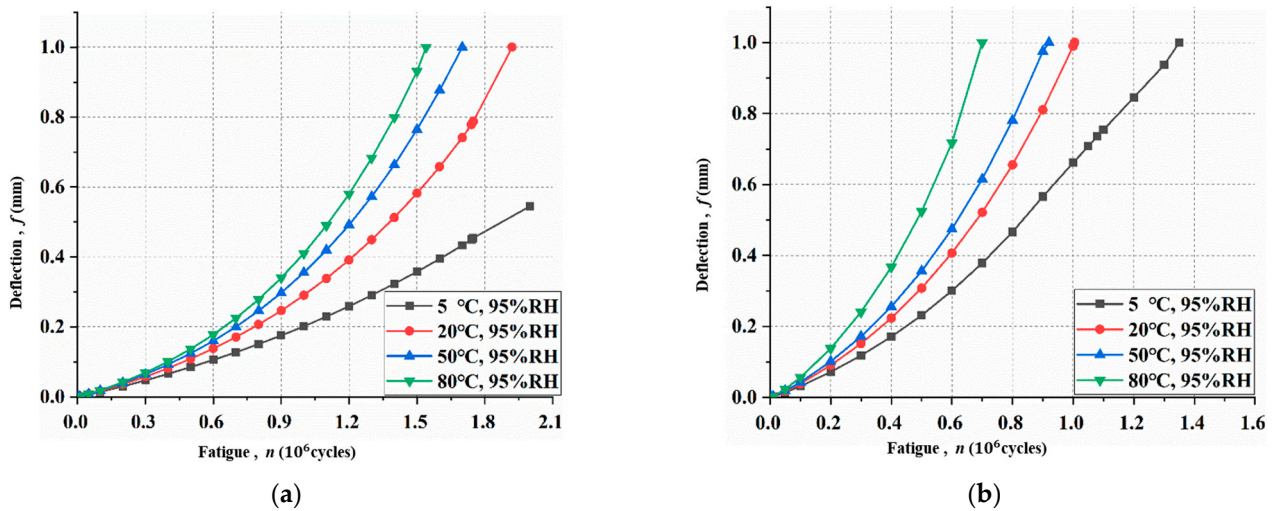


Figure 6. Cumulative damage of rebar under different hygrothermal environments at different loading levels: (a) 27.5 kN; (b) 30.0 kN.

3.3. Shear Stress Distribution

Figure 7 shows the mid-span deflections versus loading cycles under different hygrothermal environments before D_s reaches 1. Under the same environment, the tensile stress of CFRP at the mid-span section increases as loading level increases. This phenomenon is due to the elastic-plastic characteristics of rebar and intermediate crack propagation; CFRP should endure more loads.

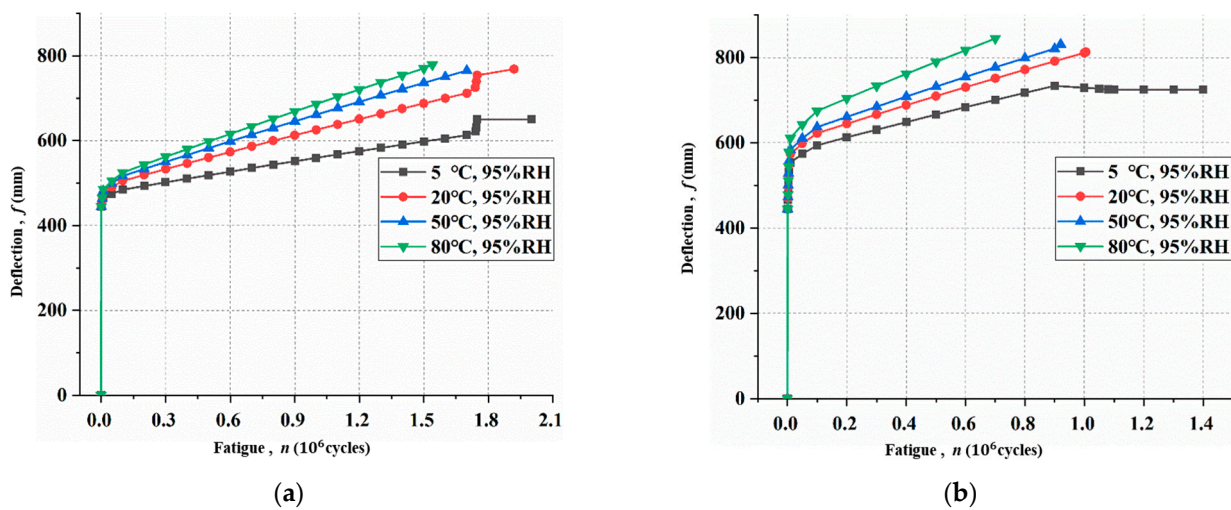


Figure 7. The tensile stress of CFRP under different hygrothermal environments at different loading levels: (a) 27.5 kN; (b) 30.0 kN.

Under the same loading level, the CFRP tensile stress increases with the temperature increase. At the loading level of 27.5 kN, the tensile stress of CFRP at 80 °C, 95% R·H increased by 33% compared with that at 5 °C, 95% R·H. When the loading level was 30 kN, the tensile stress of CFRP at 80 °C, 95% R·H increased by 21% compared with that at 5 °C, 95% R·H when D_s reached 1. The calculation results show that the high-temperature and -humidity environment has a significant effect on the tensile stress of CFRP, which is mainly due to its great influence on the bond behavior.

Based on the calculation procedure, the shear stress distribution τ and the energy release rate G_R of the CFRP–concrete interface can be obtained. Figure 8 shows the shear stress distribution along with the CFRP–concrete interface under different hygrothermal

environments when D_b reaches 1. In Figure 8, the mid-span section with intermediate bending crack is at the location of $x = 0$. The length from the mid-span with an interfacial shear stress of 0 is the debonding length and denoted by L_d . Results show that the shear stress of the interface beyond 200 mm is 0 when D_b reaches 1, and so the interfacial shear stresses beyond 200 mm have not been plotted.

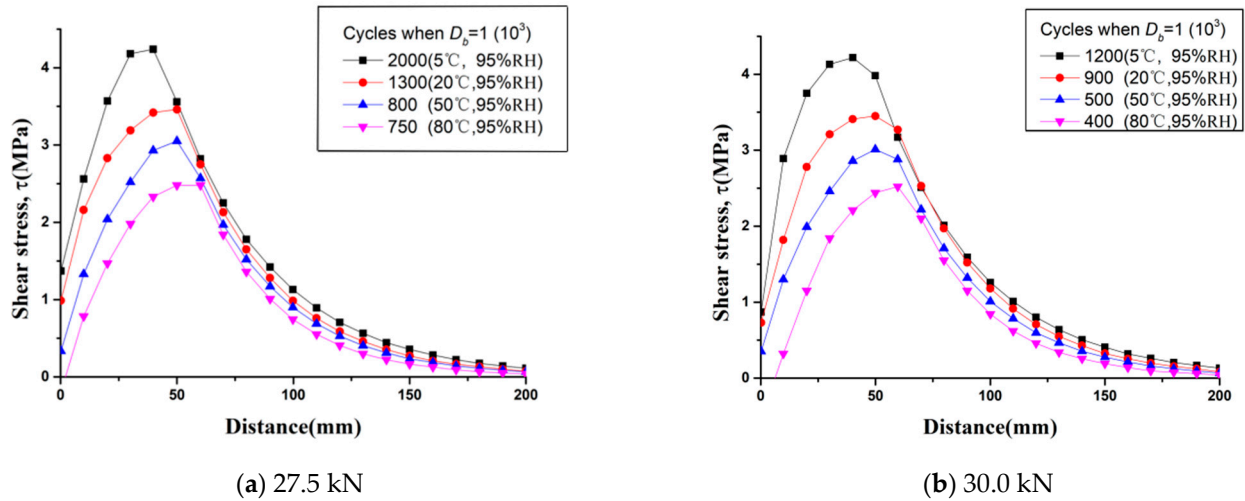


Figure 8. Shear stress distribution of CFRP–concrete interface in theory when $D_b = 1$: (a) 27.5 kN; (b) 30.0 kN.

With the comparison between the cumulative damages of rebar and the CFRP–concrete interface, the failure mode of the strengthened beam can be determined. The predicted failure modes and predicted lives of all specimens, corresponding to $D_s = 1$ and $D_b = 1$, are listed in Table 4 below.

Table 4. Detailed test information and prediction results.

Hygrothermal Environment	Specimen No.	Tested Life, N_f	Average Life, $N_{f,ave}$	Predicted Failure Mode	Predicted Life ($D_s = 1$)	Predicted Life ($D_b = 1$)
5 °C 95% R-H	A5-27.5-1	$>2 \times 10^6$	1,732,965	A	1,400,000	1,400,000
	A5-27.5-2	$>2 \times 10^6$				
	A5-30.0-1	1,465,930				
	A5-30.0-2	$>2 \times 10^6$				
20 °C 95% R-H	B20-27.5-1	1,853,118	1,227,000	B	1,920,000	1,300,000
	B20-27.5-2	521,580				
	B20-27.5-3	$>2 \times 10^6$				
	B20-27.5-4	686,534				
	B20-27.5-5	1,073,814				
	B20-30.0-1	1,007,974	869,046	B		
	B20-30.0-2	1,208,013				
	B20-30.0-3	711,981				
B20-30.0-4	548,219					
50 °C 95% R-H	C50-27.5-1	654,546	699,349	B	1,760,000	800,000
	C50-27.5-2	1,190,746				
	C50-27.5-3	252,756				
	C50-30.0-1	407,828	454,307			
	C50-30.0-2	600,001				
	C50-30.0-3	355,094				
80 °C 95% R-H	D80-27.5-1	188,882	790,312	B	1,600,000	750,000
	D80-27.5-2	702,624				
	D80-27.5-3	1,479,430				
	D80-30.0-1	140,175	388,166			
	D80-30.0-2	127,738				
	D80-30.0-3	896,585				

Note: the first part of Specimen No. refers to the environment group; the second is the peak load, and the third is the serial number. Failure mode A refers to rebar rupture and B refers to IC debonding failure.

predicted results. The maximum relative error is 19.2% compared with the average test results. For the fatigue lives at a loading level of 30 kN, the relative error is 4.2% in the case of IC debonding failure. However, there is a large relative error of 63% in the case of rebar rupture. Therefore, the failure of IC debonding should be taken into consideration when CFRP-strengthened RC beams are subjected to high-level fatigue loads.

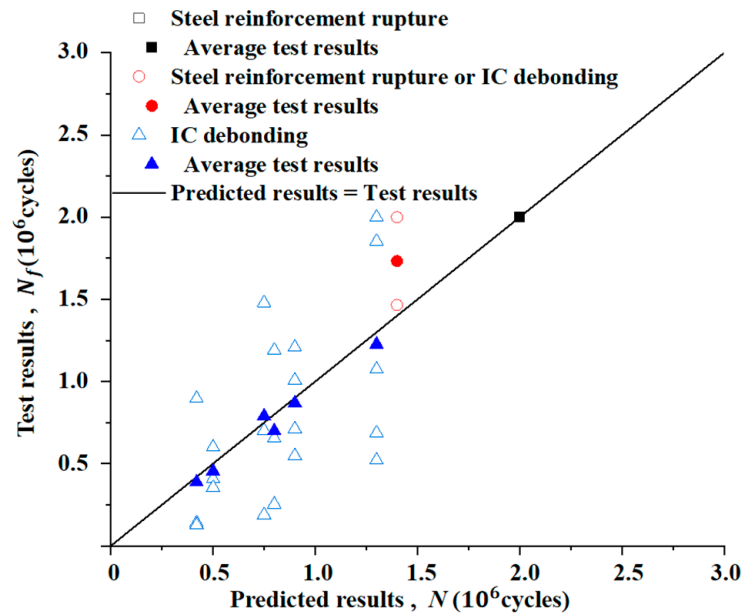


Figure 10. Comparison of the tested and predicted fatigue lives.

5. Conclusions

A fatigue life prediction model for CFRP-strengthened RC beams under hygrothermal environments was proposed, with consideration of the interfacial characters of CFRP–concrete. Corresponding failure criteria for rebar fracture and IC debonding were established. The proposed model can be used to analyze the fatigue behavior of strengthened beams and provide a scientific basis for life evaluation and retrofit design of RC bridges. The following conclusions have been drawn:

Flexural concrete cracks grew rapidly and remained stable, while the main crack at the mid-span section continued to propagate and caused damage accumulated in rebars. The performance of concrete and the CFRP–concrete interface degraded under fatigue loads and hygrothermal conditions, leading to increases in crack length and deflection.

The behavior of the CFRP–concrete interface degraded significantly under hygrothermal environments. When the strengthened beam was subjected to low-temperature conditions, the test failure mode was rebar rupture, which agreed with the model prediction. In the case of high-temperature conditions, the failure mode changed to IC debonding, which was also successfully predicted.

The interfacial shear stress exhibited a large increase under a high loading level, leading to IC debonding failure. The accuracy of fatigue life prediction was enhanced with the consideration of failure modes.

Fatigue life prediction matched the average test results well, but there were errors caused by specimen discreteness. Further research will be focused on FEM simulation, which will be helpful for improving the proposed model.

Author Contributions: Data curation, X.G. and Y.W.; Formal analysis, Z.C.; Funding acquisition, X.G.; Investigation, X.G., H.C. and Y.W.; Methodology, Z.C.; Visualization, H.C. and Y.W.; Writing—original draft, X.G. and H.C.; Writing—review & editing, Z.C. All authors have read and agreed to the published version of the manuscript.

Funding: The research was funded by the National Natural Science Foundation of China (Nos. 12172134, 11872185).

Institutional Review Board Statement: Not applicable.

Informed Consent Statement: Not applicable.

Data Availability Statement: The data presented in this study are available on request from the corresponding author.

Conflicts of Interest: The authors declare no conflict of interest.

References

1. Chen, Z.-B.; Huang, P.-Y.; Li, Z.-W.; Guo, X.-Y.; Zhao, C.; Zheng, X.-H.; Yang, Y. Fatigue Performance of RC Beams Strengthened with CFRP under Overloads with a Ladder Spectrum. *Sensors* **2018**, *18*, 3321. [[CrossRef](#)] [[PubMed](#)]
2. Wysmulski, P.; Debski, H.; Falkowicz, K.; Rozylo, P. The influence of load eccentricity on the behavior of thin-walled compressed composite structures. *Compos. Struct.* **2019**, *213*, 98–107. [[CrossRef](#)]
3. Rozylo, P. Stability and failure of compressed thin-walled composite columns using experimental tests and advanced numerical damage models. *Int. J. Numer. Methods Eng.* **2021**, *122*, 5076–5099. [[CrossRef](#)]
4. Rougier, V.C.; Luccioni, B.M. Numerical assessment of FRP retrofitting systems for reinforced concrete elements. *Eng. Struct.* **2007**, *29*, 1664–1675. [[CrossRef](#)]
5. Elsayed, W.; Ebead, U.A.; Neale, K.W. Interfacial behavior and debonding failures in FRP-strengthened concrete slabs. *J. Compos. Constr.* **2007**, *11*, 619–628. [[CrossRef](#)]
6. Dong, J.F.; Wang, Q.Y.; Guan, Z.W. Structural behaviour of RC beams externally strengthened with FRP sheets under fatigue and monotonic loading. *Eng. Struct.* **2012**, *41*, 24–33. [[CrossRef](#)]
7. Charalambidi, B.G.; Rousakis, T.C.; Karabinis, A.I. Fatigue Behavior of Large-Scale Reinforced Concrete Beams Strengthened in Flexure with Fiber-Reinforced Polymer Laminates. *J. Compos. Constr.* **2016**, *20*, 04016035. [[CrossRef](#)]
8. Al-Rousan, R.; Issa, M. Fatigue performance of reinforced concrete beams strengthened with CFRP sheets. *Constr. Build. Mater.* **2011**, *25*, 3520–3529. [[CrossRef](#)]
9. Papaconstantinou, C.; Balaguru, P.; Petrou, M. Analysis of reinforced concrete beams strengthened with composites subjected to fatigue loading. *Concr. Mater. Sci. Appl.* **2002**, *206*, 41–60.
10. Ferrier, E.; Bigaud, D.; Clément, J.C.; Hamelin, P. Fatigue-loading effect on RC beams strengthened with externally bonded FRP. *Constr. Build. Mater.* **2011**, *25*, 539–546. [[CrossRef](#)]
11. Ferrier, E.; Quiertant, M.; Benzarti, K.; Hamelin, P. Influence of the properties of externally bonded CFRP on the shear behavior of concrete/composite adhesive joints. *Compos. Part B-Eng.* **2010**, *41*, 354–362. [[CrossRef](#)]
12. Chen, G.M.; Chen, J.F.; Teng, J.G. Behaviour of FRP-to-concrete interfaces between two adjacent cracks: A numerical investigation on the effect of bondline damage. *Constr. Build. Mater.* **2012**, *28*, 584–591. [[CrossRef](#)]
13. Zhou, Y.; Chen, X.; Fan, Z.; Sui, L.; Li, D.; Xing, F. Bond behaviors of FRP-to-concrete interface under the control of a novel end-anchorage system. *Compos. Struct.* **2017**, *168*, 130–142. [[CrossRef](#)]
14. Dai, J.; Ueda, T.; Sato, Y. Development of the Nonlinear Bond Stress-Slip Model of Fiber Reinforced Plastics Sheet-Concrete Interfaces with a Simple Method. *J. Compos. Constr.* **2005**, *9*, 52–62. [[CrossRef](#)]
15. Lu, X.Z.; Teng, J.G.; Ye, L.P.; Jiang, J.J. Bond-slip models for FRP sheets/plates bonded to concrete. *Eng. Struct.* **2005**, *27*, 920–937. [[CrossRef](#)]
16. Ferracuti, B.; Savoia, M.; Mazzotti, C. Interface law for FRP-concrete delamination. *Compos. Struct.* **2007**, *80*, 523–531. [[CrossRef](#)]
17. Ko, H.; Matthys, S.; Palmieri, A.; Sato, Y. Development of a simplified bond stress-slip model for bonded FRP-concrete interfaces. *Constr. Build. Mater.* **2014**, *68*, 142–157. [[CrossRef](#)]
18. Al-Saoudi, A.; Al-Mahaidi, R.; Kalfat, R.; Cervenka, J. Finite element investigation of the fatigue performance of FRP laminates bonded to concrete. *Compos. Struct.* **2019**, *208*, 322–337. [[CrossRef](#)]
19. Wang, Y.L.; Guo, X.Y.; Huang, P.Y.; Huang, K.N.; Yang, Y.; Chen, Z.B. Finite element investigation of fatigue performance of CFRP-strengthened beams in hygrothermal environments. *Compos. Struct.* **2020**, *234*, 111676. [[CrossRef](#)]
20. Loo, K.Y.M.; Foster, S.J.; Smith, S.T. FE Modeling of CFRP-Repaired RC Beams Subjected to Fatigue Loading. *J. Compos. Constr.* **2012**, *16*, 572–580. [[CrossRef](#)]
21. Oudah, F.; El-Hacha, R. Research progress on the fatigue performance of RC beams strengthened in flexure using Fiber Reinforced Polymers. *Compos. Part B-Eng.* **2013**, *47*, 82–95. [[CrossRef](#)]
22. Diab, H.; Wu, Z. A linear viscoelastic model for interfacial long-term behavior of FRP-concrete interface. *Compos. Part B-Eng.* **2008**, *39*, 722–730. [[CrossRef](#)]
23. Biscaia, H.C.; Silva, M.A.G.; Chastre, C. An experimental study of GFRP-to-concrete interfaces submitted to humidity cycles. *Compos. Struct.* **2014**, *110*, 354–368. [[CrossRef](#)]
24. Mukherjee, A.; Arwihar, S.J. Performance of externally bonded GFRP sheets on concrete in tropical environments. Part I: Structural scale tests. *Compos. Struct.* **2007**, *81*, 21–32. [[CrossRef](#)]

25. Haber, Z.B.; Mackie, K.R.; Zhao, L. Mechanical and environmental loading of concrete beams strengthened with epoxy and polyurethane matrix carbon fiber laminates. *Constr. Build. Mater.* **2012**, *26*, 604–612. [[CrossRef](#)]
26. Subramaniam, K.V.; Ali-Ahmad, M.; Ghosn, M. Freeze–thaw degradation of FRP–concrete interface: Impact on cohesive fracture response. *Eng Fract Mech.* **2008**, *75*, 3924–3940. [[CrossRef](#)]
27. Ekenel, M.; Myers, J.J. Fatigue performance of CFRP strengthened RC beams under environmental conditioning and sustained load. *J. Compos. Constr.* **2009**, *13*, 93–102. [[CrossRef](#)]
28. Soudki, K.; El-Salakawy, E.; Craig, B. Behavior of CFRP strengthened reinforced concrete beams in corrosive environment. *J. Compos. Constr.* **2007**, *11*, 291–298. [[CrossRef](#)]
29. Aiello, M.; Frigione, M.; Leone, M.; Aniskevich, A. Effect of temperature on mechanical performances of CFRP rebars. In Proceedings of the 24th International SAMPE Europe Conference of the Society for the Advancement of Material and Process Engineering, Paris, France, 1–3 April 2003; pp. 239–249.
30. Zheng, X.H.; Huang, P.Y.; Chen, G.M.; Tan, X.M. Fatigue behavior of FRP–concrete bond under hygrothermal environment. *Constr. Build. Mater.* **2015**, *95*, 898–909. [[CrossRef](#)]
31. Leone, M.; Matthys, S.; Aiello, M.A. Effect of elevated service temperature on bond between FRP EBR systems and concrete. *Compos. Part B-Eng.* **2009**, *40*, 85–93. [[CrossRef](#)]
32. Dai, J.-G.; Gao, W.; Teng, J. Bond-slip model for FRP laminates externally bonded to concrete at elevated temperature. *J. Compos. Constr.* **2013**, *17*, 217–228. [[CrossRef](#)]
33. Huang, P.-Y.; Zhou, H.; Wang, H.-Y.; Guo, X.-Y. Fatigue lives of RC beams strengthened with CFRP at different temperatures under cyclic bending loads. *Fatigue Fract. Eng. M.* **2011**, *34*, 708–716. [[CrossRef](#)]
34. Qin, G.; Huang, P.; Zhou, H.; Guo, X.; Zheng, X. Fatigue and durability behavior of RC beams strengthened with CFRP under hot-wet environment. *Constr. Build. Mater.* **2016**, *111*, 735–742. [[CrossRef](#)]
35. Guo, X.; Huang, P.; Wang, Y.; Shu, S.; Zheng, X. Flexural Performance of Reinforced Concrete Beams Strengthened with Carbon Fiber-Reinforced Polymer (CFRP) under Hygrothermal Environment Considering the Influence of CFRP–Concrete Interface. *Acta Mech. Solida Sin.* **2021**, *34*, 381–392. [[CrossRef](#)]
36. Popovics, S. A numerical approach to the complete stress-strain curve of concrete. *Cem. Concr. Res.* **1973**, *3*, 583–599. [[CrossRef](#)]
37. Zheng, X. *Study on the Bond-Slip Mechanism of CFL-Concrete Interface under Hot-Wet Environment*; South China University of Technology: Guangzhou, China, 2014. (In Chinese)
38. Holmen, J.O. Fatigue of concrete by constant and variable amplitude loading. *Fatigue Concr. Struct.* **1982**, *75*, 71–110.
39. Song, Y.; Wang, H.; Jia, J. Behavior of concrete under multi-axial fatigue loading. *J. Build. Struct.* **2008**, *29*, 260–265.
40. Meier, U.; Nishibayashi, S.; Kuroda, T.; Omata, F. Fatigue strength and deformation characteristics of reinforced concrete beams strengthened with carbon fiber-reinforce plastic plate. *Trans. Jpn. Concr. Inst.* **1995**, *17*, 149–156.
41. Aidoo, J.; Harries, K.A.; Petrou, M.F. Fatigue behavior of carbon fiber reinforced polymer-strengthened reinforced concrete bridge girders. *J. Compos. Constr.* **2004**, *8*, 501–509. [[CrossRef](#)]
42. Heffernan, P.; Erki, M. Fatigue behavior of reinforced concrete beams strengthened with carbon fiber reinforced plastic laminates. *J. Compos. Constr.* **2004**, *8*, 132–140. [[CrossRef](#)]
43. Wang, X.; Sayed, A.M.; Wu, Z. Modeling of the flexural fatigue capacity of RC beams strengthened with FRP sheets based on finite-element simulation. *J. Struct. Eng.* **2015**, *141*, 04014189. [[CrossRef](#)]
44. De Lorenzis, L. *Strengthening of RC Structures with near Surface Mounted FRP Rods*; Department of Civil Engineering, University of Missouri-Rolla: Rolla, MO, USA, 2000.
45. Hoque, N.; Jumaat, M.; Sulong, N. Global Energy Balance–Based Debonding Modeling of NSM FRP-Strengthened Concrete Beam. *J. Compos. Constr.* **2020**, *24*, 04019053. [[CrossRef](#)]
46. Chen, Z.; Huang, P.; Yao, G.; Guo, X.; Yang, Y.; Li, W.; Wu, B. Experimental study on fatigue performance of RC beams strengthened with CFRP under variable amplitude overload and hot-wet environment. *Compos. Struct.* **2020**, *244*, 112308. [[CrossRef](#)]